Cellular/Molecular

Boosting of Action Potential Backpropagation by Neocortical Network Activity *In Vivo*

Jack Waters and Fritjof Helmchen
Abteilung Zellphysiologie, Max-Planck-Institut für medizinische Forschung, 69120 Heidelberg, Germany

Action potentials backpropagate into the dendritic trees of pyramidal neurons, reporting output activity to the sites of synaptic input and provoking long-lasting changes in synaptic strength. It is unclear how this retrograde signal is modified by neural network activity. Using whole-cell recordings from somata, apical trunks, and dendritic tuft branches of layer 2/3 pyramidal neurons *in vivo*, we show that network-driven subthreshold membrane depolarizations ("up states") occur simultaneously throughout the apical dendritic tree. This spontaneous synaptic activity enhances action potential-evoked calcium influx into the distal apical dendrite by promoting action potential backpropagation. Hence, somatic feedback to the dendrites becomes stronger with increasing network activity.

Key words: **dendrite; two-photon; calcium; layer 2/3; up state; pyramidal neuron**

Introduction

How does a neuron translate the many synaptic inputs arriving in its dendritic tree into the pattern of action potentials that form its output? In pyramidal neurons, synaptic inputs are integrated both locally, in the dendrites, and at the site of action potential (AP) initiation in the axon initial segment. Local, dendritic integration relies on nonlinear, active properties, which depend on voltage-sensitive ion channels in the dendritic membrane (Reyes, 2001; Migliore and Shepherd, 2002). Active properties include dendritic spike initiation and backpropagation of axosomatically generated APs into the dendritic tree (Stuart and Sakmann, 1994; Stuart et al., 1997a,b; Häusser et al., 2000; Waters et al., 2005). AP backpropagation is a retrograde signaling mechanism that reports spike output to the dendrites, promotes dendritic calcium influx, and thereby enables Hebbian synaptic plasticity based on the coincidence of APs and synaptic input (Sjöström and Nelson, 2002).

In pyramidal neurons, backpropagating APs are supported by dendritic sodium channels. The amplitude of an AP nonetheless decreases as it backpropagates into the dendritic tree (Stuart and Sakmann, 1994; Stuart et al., 1997b; Waters et al., 2005). In layer 2/3 (L2/3) pyramidal neurons, we recently demonstrated that this decremental attenuation and the resulting spatial profile of dendritic calcium influx are similar in brain slices and during periods of little spontaneous synaptic activity in the intact brain (*in vivo*; Waters et al., 2003). However, the neocortex is spontaneously active. For example, spontaneous fluctuations in postsynaptic membrane potential occur during slow-wave sleep and under anesthesia. These are commonly referred to as "up" and "down" states and reflect periods of pronounced and reduced synaptic activity, respectively (Steriade et al., 1993; Cowan and Wilson, 1994; Timofeev et al., 2001). Neurons are therefore subjected to prolonged periods of pronounced synaptic input, caused by both spontaneous and evoked network activity (Destexhe et al., 2003). Studies of brain slice preparations indicate that the degree of AP attenuation in the dendrite depends on coincident synaptic input. Backpropagating APs can be boosted or suppressed by excitatory and inhibitory input, respectively (Tsubokawa and Ross, 1996; Magee and Johnston, 1997; Stuart and Häusser, 2001; Xiong and Chen, 2002; Bernard and Johnston, 2003). It is therefore unclear how AP backpropagation is altered when the surrounding network is active *in vivo*.

Here we examine the impact of spontaneous cortical activity on dendritic integration using whole-cell recording and two-photon calcium imaging from layer 2/3 neurons in the barrel cortex of anesthetized rats. First we demonstrate that the entire apical dendrite receives synaptic input during up states. We then show that both spontaneous and evoked synaptic activity increase AP-evoked calcium influx into the distal apical dendritic tree by boosting AP backpropagation.

Materials and Methods

Animal preparation. Four-week-old [postnatal day 27 (P27)–P32] Wistar rats were anesthetized with urethane (1–2 gm/kg, i.p.). Depth of anesthesia was sufficient to eliminate pinch withdrawal, corneal reflex, and vibrissal movements. A small (2 × 2 mm) craniotomy was opened over barrel cortex (centered 2 mm posterior to bregma, 5–6 mm lateral), and the dura was removed. The craniotomy was covered with agar (1–1.5%, type III-A; Sigma, St. Louis, MO) in the following solution (in mM): 135 NaCl, 5.4 KCl, 1 $MgCl_2$, 1.8 $CaCl_2$, and 5 HEPES. A glass coverslip was positioned over the agar. Gentle downward pressure was applied to the coverslip to reduce heartbeat and breathing-induced motion of the cortex (Svoboda et al., 1999b). All experimental procedures were performed in accordance with the animal welfare guidelines of the Max Planck Society.

Received July 20, 2004; revised Oct. 21, 2004; accepted Oct. 22, 2004.

This work was supported by the Max-Planck-Gesellschaft and by a Marie Curie individual fellowship from the European Union to J.W. (contract number QLGA-CT-2001-50999). We thank Bert Sakmann for his generous support, Marlies Kaiser for expert technical assistance, and Damian Haydon-Wallace, Jason Kerr, Michael Becht, Pavel Osten, and Verena Pawlak for comments on this manuscript.

Correspondence should be addressed to Jack Waters, Abteilung Zellphysiologie, Max-Planck-Institut für medizinische Forschung, Jahnstrasse 29, 69120 Heidelberg, Germany. E-mail: jwaters@mpimf-heidelberg.mpg.de.

DOI:10.1523/JNEUROSCI.2933-04.2004

 0270-6474/04/2411127-10$15.00/0

Electrophysiology. Whole-cell patch-clamp recordings were obtained using a "blind" technique as described previously (Margrie et al., 2002). Somatic and trunk recordings were obtained using pipettes with 4–6 MΩ tip resistance. For tuft recordings we used sharper pipettes (10–25 MΩ) and searched only in layer 1. All recording pipettes were filled with an intracellular solution containing: 135 mM K-gluconate, 4 mM KCl, 10 mM HEPES, 10 mM Na_2-phosphocreatine, 4 mM Mg-ATP, 300 μM Na-GTP, 200 μM Oregon Green BAPTA 488–1 (OGB-1), 20 μM Alexa 594, and 0.2% (w/v) biocytin, pH 7.2; 291–293 mOsm. Positive pressure (200–400 mbar) was applied to the pipette as it was inserted through the agar and the pial surface of the cortex. The positive pressure was reduced to 25–30 mbar when the tip was at approximately the upper border of L2/3 (for somatic recordings) or ~20 μm below the pia (for dendritic tuft recordings). The pipette was then advanced in 2 μm steps. Voltage pulses were applied to the pipette (10–20 mV, 30 msec, 10 Hz), and the current response was monitored. Positive pressure was relieved when the series resistance of the electrode abruptly increased immediately after a 2 μm step, indicating that the tip of the pipette may have been pushed against a neuronal plasma membrane. Gentle suction (up to 100 mbar) was applied where necessary to obtain a gigaohm seal. Initial access resistances were typically 30–60 MΩ at the soma and 100–200 MΩ in the dendritic tuft branches. All recordings were obtained using an Axoclamp-2B amplifier (Axon Instruments, Union City, CA).

L2/3 pyramidal neurons were identified in somatic recordings by (1) their regular firing pattern, (2) their characteristic apical dendrite and distal tuft, and (3) the depth of the soma below the pia (150–500 μm) measured using the two-photon microscope. In dendritic recordings, only the latter two criteria were applied. Every neuron responded to whisker stimulation (air-puff) with a 5–15 mV EPSP, confirming that all recordings were obtained from barrel cortex. The recording site was located by focusing down into the brain from the pial surface using the fluorescent image of the dye-filled electrode as a guide.

For electrocorticogram (ECoG) recordings, the tip of a 75 μm diameter, Teflon-coated silver wire was placed against the pial surface in one corner of the craniotomy. A reference electrode, made from similar or larger diameter wire, was placed in a small hole over the cerebellum and immobilized with dental acrylic. ECoG signals were acquired using a custom-built AC-coupled amplifier (input impedance 1 MΩ; bandwidth 0.1 Hz to 8 kHz). Both ECoG and membrane potential were sampled at 10 kHz using an 16-bit analog-to-digital converter (ITC-16, Instrutech, Great Neck, NY) and custom-written acquisition software (IGOR; Wavemetrics, Eugene, OR).

Extracellular stimulation was performed using a coated tungsten electrode (part number TM31A10KT; shaft diameter, 216 μm; tip diameter, 1 μm; impedance, ~1 MΩ; Parylene-C coating; WPI, Sarasota, FL). The stimulation electrode was mounted on a manipulator, inserted under the glass coverslip, and pushed through the agar and into layer 1. These electrodes are fluorescent, which allowed us to consistently place the tip of the electrode 50–100 μm below the pial surface under visual guidance. Stimulus strength was adjusted to be just sufficient to evoke a single AP (1 msec pulses; intensity range, 2–900 μA).

Two-photon microscopy. In vivo Ca^{2+} imaging was combined with whole-cell recordings as described previously (Svoboda et al., 1999b; Helmchen and Waters, 2002). A custom-built two-photon microscope was used. Excitation light at a center wavelength of 840 nm was provided by a pulsed Ti:sapphire laser (80 MHz repetition rate; 100–150 fsec pulse width; Mira 900, Coherent, Santa Clara, CA) pumped by a 10 W solid-state laser (Verdi-V10; Coherent). Excitation light was focused onto the specimen using a 40× water immersion objective (numerical aperture 0.8; Zeiss, Oberkochen, Germany). Emitted fluorescence was deflected by a 680 nm long-pass dichroic mirror positioned close to the objective and then separated into a "green" and a "red" channel using a long-pass dichroic mirror (570 DCXR; AHF Analysentechnik). Emission filters were BG39 color glass and a HQ610/75M bandpass filter for the green and red channel, respectively. Infrared stray light was blocked using an infrared blocking filter (Calflex; Linos, Milford, MA). Fluorescence was detected with photomultiplier tubes (R6357; Hamamatsu, Tokyo, Japan). Mirror scanning and image acquisition were controlled using custom software (R. Stepnoski and M. Müller, Lucent Technologies, MPImF, Heidelberg, Germany).

To identify and visualize neuronal morphology, high-resolution fluorescence image stacks were acquired at the end of each experiment (256 × 256 pixel images; several hundred focal planes at 2 μm increments). From these stacks two-photon side projections were calculated as maximum intensity projections. Single AP-evoked dendritic fluorescence transients were measured using 64-pixel linescans at 500 Hz. Fluorescence was averaged over the width of the dendrite and expressed as relative fluorescence change ($\Delta F/F$) after subtraction of background fluorescence from an adjacent region. Fluorescence traces were smoothed in the temporal domain using a 3- to 5-point Gaussian filter. Peak $\Delta F/F$ amplitudes were determined by fitting the decaying phase of the Ca^{2+} transient with a single exponential curve and back-extrapolating this fit to the time point corresponding to the start of the fluorescence transient.

Histology. After experiments, animals were transcardially perfused with 4% paraformaldehyde in phosphate buffer (in mM: 75 Na_2HPO_4 and 25 NaH_2PO_4, pH 7.2). The brain was removed and stored for 2 d at 4°C in the same solution. Intracellular biocytin was visualized using the avidin–biotin horseradish peroxidase reaction and 3,3-diaminobenzidine (DAB) as described previously (Lübke et al., 2000). Neuronal morphologies were reconstructed using Neurolucida software (MicroBrightField, Colchester, VT).

Data analysis. Mean membrane potentials during down and up states were defined as the modal values of the two peaks in the membrane potential frequency histograms (bin width, 1 mV). To compare intracellular whole-cell recordings with the ECoG (see Fig. 3), the membrane potential traces were smoothed using a binomial low-pass filter (17 Hz cutoff frequency) and then differentiated. The cross-correlation $h(\tau)$ between the ECoG and first derivative of the membrane potential was calculated using the following equation (Lampl et al., 1999):

$$h(\tau) = \frac{\sum_{t=-n}^{n} (x_t - \bar{x})(y_{t+\tau} - \bar{y})}{\sqrt{\sum_{t=-n}^{n} (x_t - \bar{x})^2 \sum_{t=-n}^{n} (y_t - \bar{y})^2}}, \quad (1)$$

where x and y are the V_m and ECoG signal, respectively, and $2n + 1$ is the number of samples in each trace. From this equation, two identical waves (or scaled versions) would give a cross-correlation of one at zero time lag ($\tau = 0$). Mean cross-correlograms for multiple cells were obtained by averaging the cross-correlograms from individual cells (see Fig. 3*E*).

Further analysis of the membrane potential fluctuations was performed in the frequency domain (see Fig. 2*B–D*). Power spectra of the membrane potential traces were analyzed using IGOR software (Wavemetrics). Time-frequency spectrograms were calculated for 100 msec data segments using Hanning windowing ("Bsound" procedures for IGOR written by B. S. Nelson, available at http://homepage.mac.com/bsnelson/BSound.html). Intensities in the spectrograms are shown on a logarithmic scale from −61 to −24 dB. Spectra were calculated for 200 msec sections of the voltage traces using Hanning-windowing. Power spectral densities (PSDs) were obtained by dividing the squares of the magnitudes by the frequency bin size. Spectral power and densities were averaged separately for sections of the membrane potential traces extracted during down states and up states. Total spectral power in a high (60–500 Hz) frequency band was calculated by integrating the PSD over this frequency window. There was a clear dependence of spectral power on the location of the recording site, with progressively higher spectral content with distance from the soma. We attribute this increase to a high frequency of dendritic synaptic inputs during the down state and to the faster kinetics of synaptic potentials in the dendrite (see Fig. 2*A*).

Action potential amplitudes and halfwidths were measured from threshold. For comparison of calcium transient amplitude and of AP amplitude and halfwidth during up and down states (see Figs. 6*C,D,* 8*C*), the values for all trials containing a single AP were ranked according to the prestimulus membrane potential (measured 0.5 msec before the start of the depolarizing current injection) (see Fig. 6*A*). We then divided

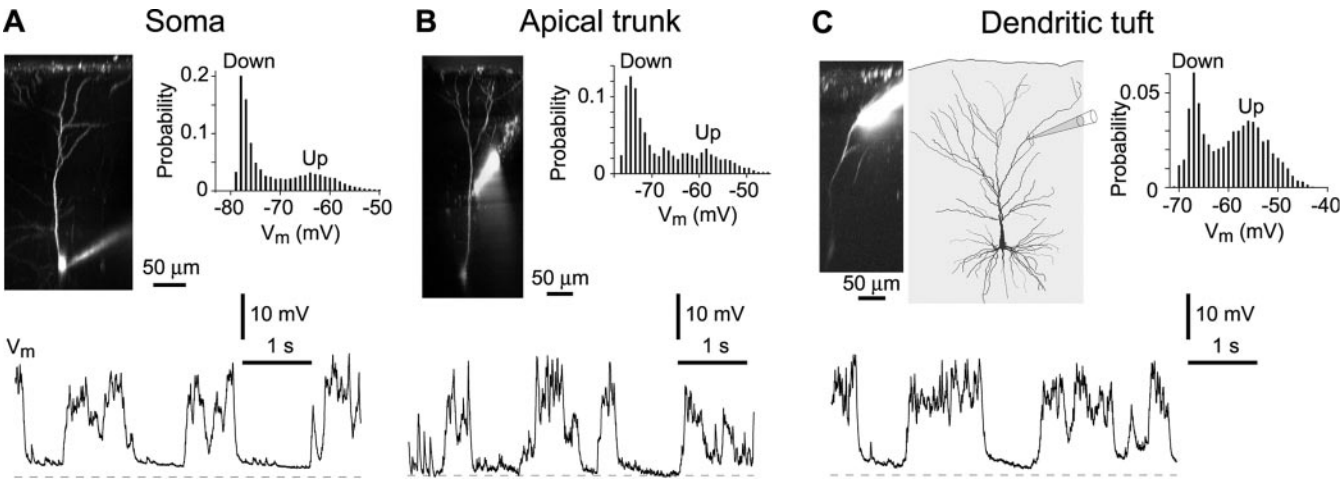

Figure 1. Dendritic recordings from L2/3 pyramidal neurons *in vivo*. Examples of recordings from the soma (*A*), the apical trunk (*B*), and the apical tuft (*C*) of L2/3 neurons are shown. Two-photon side projections (left), membrane potential (V_m) fluctuations (bottom traces), and membrane potential frequency histograms (right) are shown. Dashed lines indicate membrane potentials of −80 (*A*), −75 (*B*), and −65 (*C*) mV, respectively. The location of the whole-cell pipette is visible in the projection for each recording (*A*, soma; *B*, 170 µm from the soma; *C*, 240 µm from the soma). For the tuft recording from a secondary branch (*C*), the corresponding biocytin reconstruction is also shown.

trials into two groups: those in which the membrane potential was more hyperpolarized than the median were classified as occurring from the down state; those showing a more depolarized potential than the median were classified as occurring from the up state. Note that data points were approximately equally distributed over the voltage range in all experiments. Up and down state values were calculated as the means of these groups. Where data are presented as ratios (see Figs. 4*D*, 6*B*) the mean up state value was divided by that for the down state.

Spatial profiles of the amplitude of single AP-evoked calcium transients stimulated with an extracellular electrode were obtained by measuring the amplitudes at various dendritic locations in individual cells (supplemental Fig. 1*A*, available at www.jneurosci.org as supplemental material). Profiles were normalized to the distance between soma and pia. A skewed Gaussian curve was fit to the data using the following equation:

$$y(x) = a(x - x_0)^b e^{\left(-\frac{(x-x_0)^2}{c^2}\right)}, \quad (2)$$

where a–c, and x_0 are fitting parameters. Because of the time-consuming nature of measuring spatial profiles, we could not obtain profiles for APs evoked by current injection and by synaptic stimulation in the same cells. We therefore compared the average profile for synaptic stimulation obtained in three neurons to the average profile for current-evoked APs determined in our previous study (Waters et al., 2003) (see Fig. 7*C*) (supplemental Fig. 1*A*, available at www.jneurosci.org as supplemental material). In additional experiments we determined the ratio of the synaptically evoked calcium transient amplitude to the current-evoked amplitude at several locations in the proximal and distal apical trunk, (supplemental Fig. 1*B*, available at www.jneurosci.org as supplemental material). All distal measurements showed an increased calcium influx with synaptic stimulation (ratio >1; data points above the profile for current injection), whereas proximal measurements showed a slight decrease (ratio <1; data points below the profile for current injection). This is consistent with the extension of the profile toward the distal dendrite observed in the case of extracellular stimulation (see Fig. 7*C*).

All data are presented as mean ± SEM. All statistical tests were performed using GraphPad InStat version 3.05 software (GraphPad, San Diego, CA).

Results

Up and down states are present throughout the dendritic tree

We characterized spontaneous activity in L2/3 pyramidal neurons using recordings from the soma and throughout the dendritic tree. In somatic recordings, the membrane potential (V_m) fluctuated spontaneously between a quiescent down state (mean V_m, –73.0 ± 2.0 mV) and a more variable, depolarized up state (mean V_m, –59.9 ± 2.3 mV; $n = 11$ cells), yielding a bimodal membrane potential distribution (Fig. 1*A*). Spontaneous activity of this type has frequently been observed in somatic recordings from animals under anesthesia, during slow-wave sleep, and in some awake states (Stern et al., 1997; Lampl et al., 1999; Steriade, 2001a,b; Petersen et al., 2003). Up states, which result from waves of activity running through the cortex (Petersen et al., 2003), were eliminated by application of glutamate antagonists, but not GABA antagonists ($n = 5$ neurons, data not shown).

Up states have previously been characterized using somatic, but not dendritic recordings *in vivo*. It is therefore unclear how the synaptic inputs that drive up states are distributed over the dendritic tree. If the inputs are localized to part of the dendritic tree, their influence on synaptic integration may also be localized. To determine the distribution of synaptic inputs during up states, we obtained whole-cell recordings from apical dendrites, including the apical trunk and secondary, tertiary, and higher order tuft branches in layer 1, beyond the principal bifurcation. All recordings were obtained blind (Margrie et al., 2002), and neurons were filled with fluorescent indicators and with biocytin through the recording pipette. In somatic and trunk recordings, cellular morphology and the location of the recording site were visible in two-photon fluorescence side projections (Fig. 1*A*,*B*). In contrast, fluorescence side projections of tuft recordings often revealed only the dendritic arbor near the recording site. However, by comparison with histological reconstructions of the neurons (Fig. 1*C*), we were able to confirm that all recordings were from L2/3 neurons and to determine the locations of the recording sites.

Up and down states were clearly visible in all dendritic recordings. Membrane potential distributions from both trunk and tuft recordings were bimodal (Fig. 1*B*,*C*), and mean membrane potentials during down and up states were similar to those at the soma (–75.0 ± 2.3 and –64.0 ± 2.5 mV, $n = 8$, respectively, in apical trunk recordings and –70.4 ± 1.6 and –57.4 ± 1.7 mV, $n = 9$, in tuft recordings; no significant differences between soma and trunk or soma and tuft for either up or down states, $p > 0.1$, Mann–Whitney *U* test). Hence, the membrane potential differ-

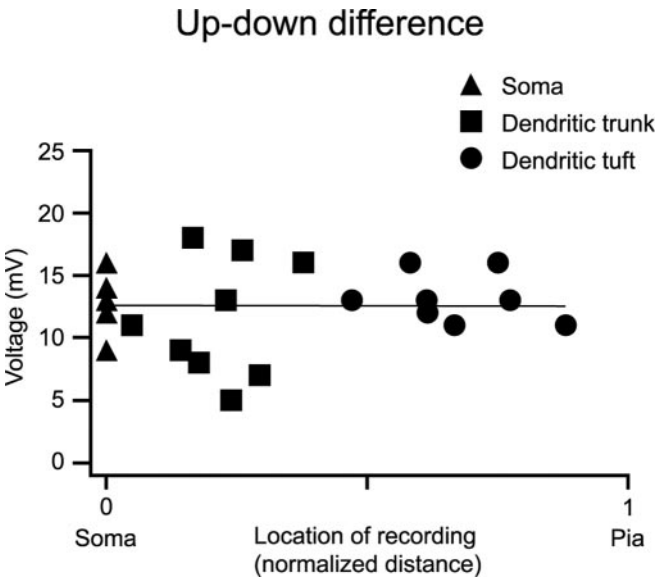

Figure 2. Up state amplitudes are similar throughout the dendritic tree. Dependence of the mean voltage difference between up and down states on the distance of the recording site from the soma is shown. Locations are normalized to the depth of the soma below the pia such that zero corresponds to the soma and one to the pia. Somatic, trunk, and tuft recordings are indicated by triangles, squares, and circles, respectively. An unconstrained linear regression line through all data points is shown.

ence between up and down states was constant along the apical dendrite from the soma to the high-order tuft dendrites (Fig. 2). If dendritic up states reflected only perisomatic input, filtered by the cable properties of the dendrite, they would be of smaller amplitude than somatic up states. Rather, our results indicate that dendritic up states reflect synaptic input distributed over the dendritic tree.

Increased synaptic input to the dendrite during the up state

Consistent with this conclusion, EPSP kinetics were faster in dendritic than in somatic recordings. EPSPs were visible during both up and down states in all recordings from tuft dendrites (Fig. 3). During down states, putative individual inputs could often be distinguished (Fig. 3*B*). In dendritic tufts, these inputs had a mean amplitude of 2.1 ± 0.2 mV (range 0.3–10 mV), a 20–80% rise time of 0.85 ± 0.08 msec, and a decay time constant of 4.5 ± 0.6 msec ($n = 192$ EPSPs from five neurons) (Fig. 3*C*). In somatic recordings, such events were less frequent and had smaller amplitudes and a slower time course (amplitude, 0.49 ± 0.03 mV, significantly smaller than in dendritic recordings, $p < 0.01$, Mann–Whitney *U* test; 20–80% rise time, 0.87 ± 0.05 msec, not significantly different from dendritic values, $p = 0.69$, Mann–Whitney *U* test; decay time constant, 10.6 ± 0.7 msec, significantly slower than in dendritic recordings, $p < 0.01$, Mann–Whitney *U* test; $n = 179$ EPSPs from five neurons) (Fig. 3*C*). The rapid time courses of the dendritic EPSPs suggest that the active synapses were close to the recording electrode.

During up states, fast EPSP-like potentials were frequently visible in tuft recordings, but large, fast membrane potential fluctuations prevented resolution of individual EPSPs (Fig. 3*B*). We therefore characterized membrane potential changes in the frequency domain (Fig. 4). Spectrograms from both somatic and dendritic recordings revealed an increase in spectral power during up states (Fig. 4*A*). At the soma, high-frequency components (more than ~60 Hz) only occurred during up states. In the dendrite, high-frequency components were present during both up and down states, but power at high frequencies nonetheless increased during up states (Fig. 4*A*). Fast EPSPs are likely to contribute substantially to the higher frequency power. Hence, our data suggest that synaptic input is increased during up states both at the soma and in the dendritic tree.

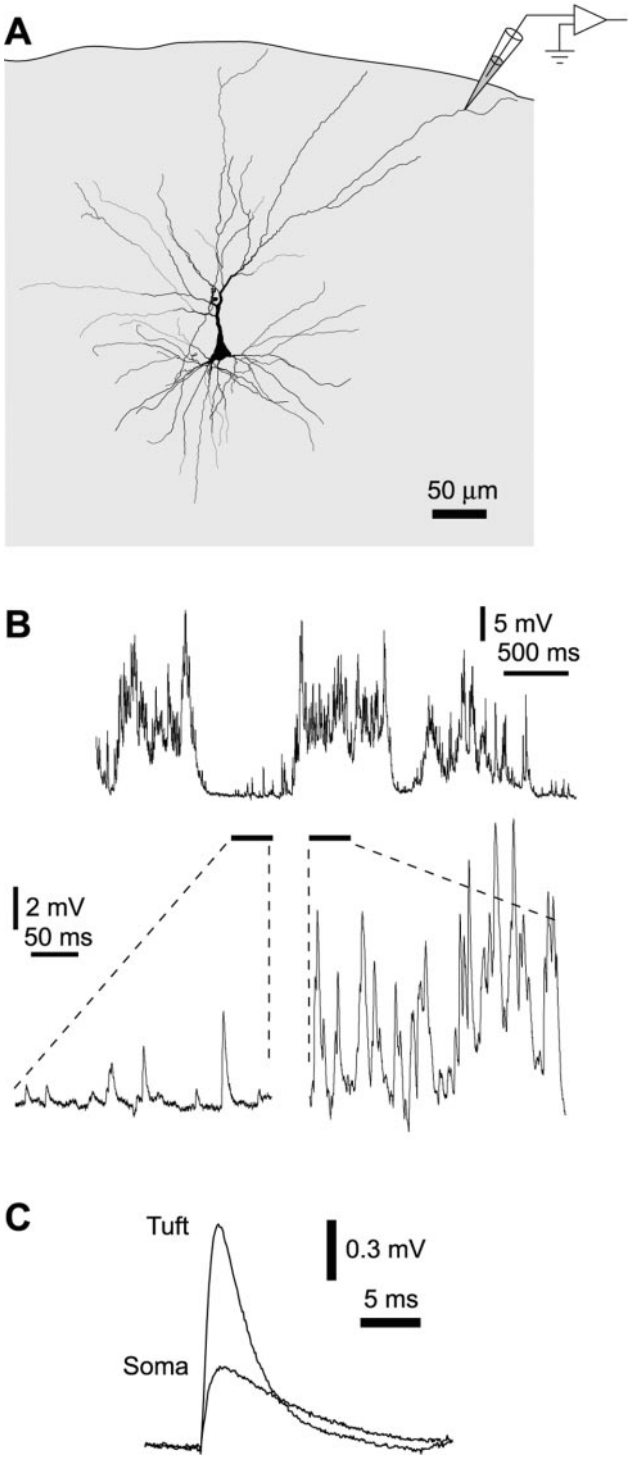

Figure 3. Synaptic input onto the dendrite during up and down states. *A,* Biocytin reconstruction of a layer 2/3 neuron, showing the location of the recording site in a quaternary dendritic tuft branch (220 µm from the soma). *B,* An example of spontaneous up states recorded in the neuron shown in *A*. Sections of the membrane potential trace during a down state and during an up state are shown on an expanded time scale (bottom). Note presumed individual EPSPs in the down state. *C,* Examples of average waveforms of EPSPs recorded from apical tuft dendrite and soma of two different neurons.

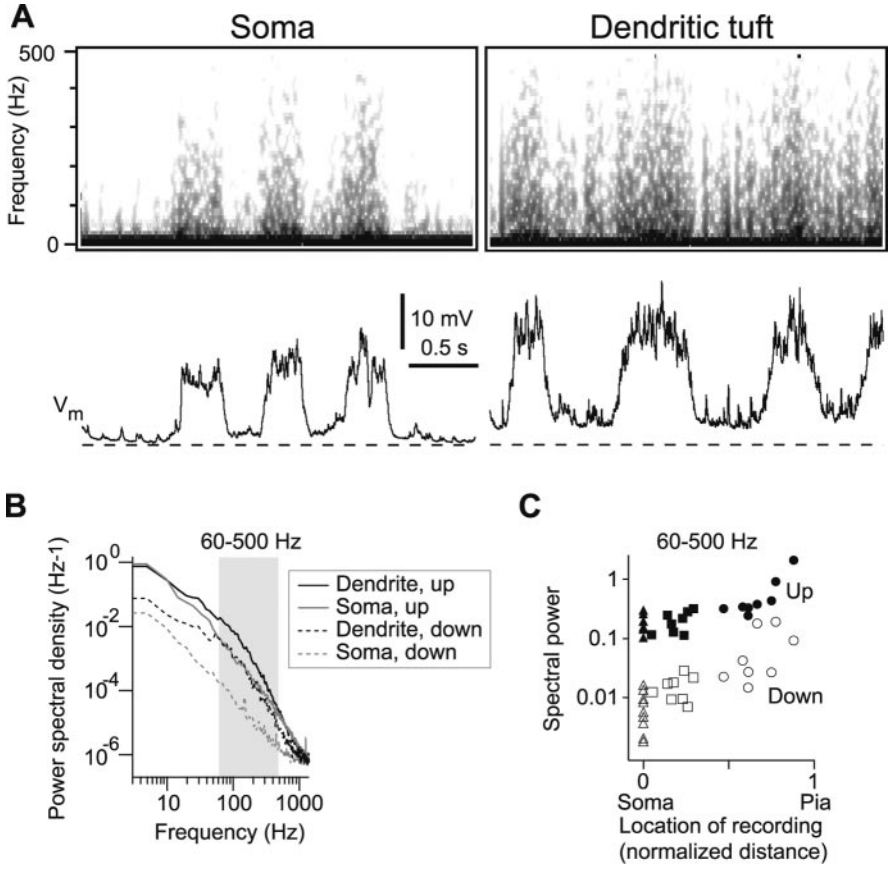

Figure 4. Spectral analysis of somatic and dendritic recordings. *A,* Examples of spontaneous membrane potential fluctuations (bottom) and the corresponding spectrograms (top) from a somatic recording (left) and from a dendritic tuft recording (right, 240 μm from the soma). Dashed lines indicate −75 mV. *B,* Power spectral densities in the soma (gray) and in the dendritic tuft (black) for the recordings shown in *B*. PSDs were computed separately for down states and up states (each averaged over 11–14 states). *C,* Spectral power in the 60–500 Hz frequency band for down states (open symbols) and up states (solid symbols) as a function of recording location. Distance is normalized to the distance between soma and pia. Somatic, trunk, and tuft recordings are indicated by triangles, squares, and circles, respectively.

We also compared high-frequency (60–500 Hz) spectral power at different recording sites (Fig. 4*B,C*). High-frequency power increased significantly with the distance of the recording site from the soma, both during down states and during up states (Fig. 4*C*) ($p < 0.001$, Spearman rank correlation). This result is consistent with the faster kinetics of EPSPs in our tuft recordings (Fig. 3*C*) and provides further evidence that synaptic input arrives throughout the dendritic tree during up states.

Up and down states are synchronized in soma and dendrite

Although we did not record simultaneously from the soma and the dendrite of an individual neuron, we were able to show that up states occur synchronously in the soma and the apical dendrite. For this purpose, we compared somatic and dendritic membrane potentials with activity in the surrounding cortical network, measured with an extracellular surface electrode. This ECoG should reflect the differential of the membrane potentials of all active neurons (Johnston and Wu, 1995). Indeed, for both somatic and dendritic recordings, the ECoG closely resembled the first-order derivative of the membrane potential (Fig. 5*A,B*). Cross-correlograms of the ECoG and the first derivative of the membrane potential had a pronounced peak at near-zero time lag (Fig. 5*C,D*). This peak was present for all somatic and dendritic recordings with combined ECoG recording and had a mean amplitude of 0.41 ± 0.01 for somatic recordings (range, 0.36–0.51; $n = 12$) and 0.33 ± 0.02 for dendritic tuft recordings (range, 0.28–0.38; $n = 4$; dendritic peak amplitude smaller than somatic peak amplitude, $p < 0.01$; Mann–Whitney *U* test) (Fig. 5*E*).

In summary, we have shown that up states occur throughout the apical dendritic tree, that they are of equal average amplitude at all locations, that the spectral power increases throughout the dendrite during up states, and that up states occur simultaneously at all locations. Together these data indicate that up states result from synaptic input arriving synchronously throughout the dendritic tree. Hence, during an up state observed at the soma, synaptic input will be increased throughout the entire apical dendritic tree.

Enhancement of AP-evoked dendritic calcium influx

We next examined the effects of these synaptic inputs on AP backpropagation into the apical dendrite. Spontaneous APs were extremely rare in dendritic recordings, as previously reported for somatic recordings (Brecht et al., 2003). However, putative backpropagating APs were observed during dendritic current injection (300–500 pA for 300 msec). Their mean amplitudes and halfwidths, measured from threshold, were 19.7 ± 2.3 mV (range 8.8–29.5; $n = 9$ neurons) and 3.2 ± 0.2 msec (range, 2.1–4.3; $n = 9$ neurons), respectively, consistent with the decremental backpropagation found in L2/3 neurons (Waters et al., 2003). Several of these putative APs occurred during up states, suggesting that AP backpropagation is maintained during up states, but we collected too few APs to compare propagation during up and down states.

We therefore used the amplitudes of AP-evoked dendritic calcium transients to reveal changes in the strength of AP backpropagation (Tsubokawa and Ross, 1996; Magee and Johnston, 1997; Xiong and Chen, 2002). In L2/3 neurons, single backpropagating APs evoke a characteristic spatial profile of dendritic calcium transient amplitudes, with a maximum in the proximal trunk, a decrease toward the principal bifurcation, and a decline to zero in the apical tuft branches (Svoboda et al., 1997, 1999a; Waters et al., 2003). We monitored calcium transients at the distal end of the apical trunk, where AP amplitudes are reduced and calcium influx is therefore particularly sensitive to the strength of AP backpropagation. If AP backpropagation is suppressed, calcium influx into the distal apical trunk is abolished (Svoboda et al., 1999a; Waters et al., 2003). In contrast, one would expect an increase in the amplitude of calcium transients at this location if AP attenuation were reduced.

Calcium transients were measured in the apical trunk, 150–175 μm from the soma, using the calcium indicator Oregon Green BAPTA-1, introduced through the recording pipette (Fig. 6*A*). Single APs were evoked by 5 msec current injections through the somatic recording pipette. Whether an AP was evoked during an up or a down state was left to chance. AP-

evoked calcium transients were sorted offline according to their prestimulus membrane potentials.

In all four neurons examined, the slope of the relationship between peak $\Delta F/F$ and prestimulus membrane potential was positive, indicating that calcium transients were larger when evoked from depolarized membrane potentials (Fig. 6*B*). The slope was significantly different from zero in two neurons ($p < 0.01$; Spearman rank correlation). The mean amplitude of the distal calcium transient was 25 ± 10% larger during up than during down states ($n = 4$ neurons) (Fig. 6*C*,*D*). Similarly, spontaneous APs (which occur only during up states) produced larger distal calcium transients than APs evoked by current injection during down states (mean amplitude 34 ± 15% larger, $n = 3$; significant difference in two of three neurons, $p < 0.05$; Mann–Whitney *U* test) (Fig. 6*D*).

The additional calcium influx does not reflect increased AP amplitude or halfwidth at the axosomatic initiation site because neither was significantly increased during up states (Fig. 6*D*) ($p > 0.5$; Mann–Whitney *U* test). It was also not caused by the prolonged depolarization associated with up states because no dendritic calcium transient was observed during subthreshold up states (Fig. 7): calcium transients occurred in the same dendritic locations only after an AP (mean peak amplitudes of 0 and 45.3 ± 8% $\Delta F/F$ for subthreshold and suprathreshold up states, respectively, $n = 9$ neurons; measurements 105–205 μm from the soma). Although localized calcium transients presumably occur close to activated synapses during up states, the additional AP-evoked calcium influx in the apical trunk was not derived from direct activation of calcium channels or NMDA receptors by synaptic input.

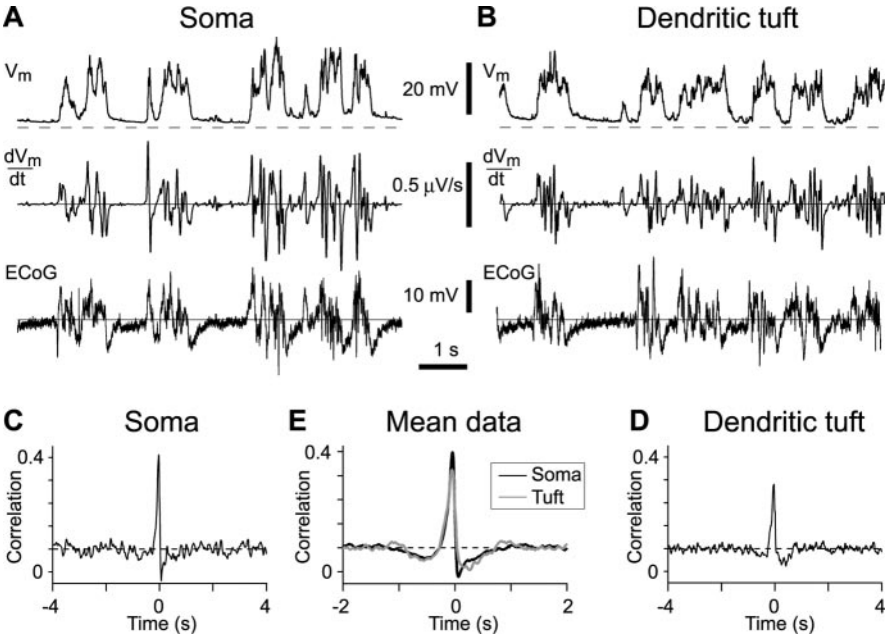

Figure 5. Up states are synchronous in somata and apical dendrites. *A, B*, Simultaneous measurements of spontaneous membrane potential fluctuations and ECoG for a somatic (*A*) and a dendritic (*B*) tuft recording. Membrane potential (V_m), first derivative of the membrane potential (dV_m/dt), and ECoG are shown. Calibration bars apply to both *A* and *B*. Dashed lines indicate membrane potentials of −80 (*A*) and −70 (*B*) mV, respectively. *C*, Cross-correlogram of the ECoG and somatic dV_m/dt for the somatic recording shown in *A*. Amplitude and position of peak, 0.40 and −32 msec. *D*, Cross-correlogram of ECoG and dendritic dV_m/dt for the tuft recording shown in *B*. Amplitude and position of peak, 0.28 and −34 msec. *E*, Mean cross-correlograms of ECoG and dV_m/dt for 12 somatic (black trace) and four dendritic tuft (gray trace) recordings. Peak amplitudes and halfwidths were 0.41 ± 0.01 and 105 msec at the soma and 0.33 ± 0.02 and 125 msec in the dendrite.

Our observation that AP-evoked dendritic calcium transients are not smaller during up states demonstrates that AP backpropagation is not suppressed by spontaneous network activity. Rather, we find that calcium influx is enhanced, suggesting that AP backpropagation may be boosted.

AP boosting by synaptic activity

Boosting of AP backpropagation by EPSPs has been described in brain slice preparations, where dendritic depolarization can enhance sodium channel activation and/or decrease potassium channel activation, leading to an increase in the dendritic amplitude of a backpropagating AP (Magee and Johnston, 1997; Pan and Colbert, 2001; Stuart and Häusser, 2001; Bernard and Johnston, 2003). This effect occurs only in the distal dendrite, where the amplitude of a backpropagating AP (in the absence of synaptic input) may be slightly below the threshold for sodium channel activation (Stuart and Häusser, 2001; Bernard and Johnston, 2003). Only a brief depolarization (such as an EPSP) is required to achieve this effect because of the rapid kinetics of sodium and potassium channels (Pan and Colbert, 2001; Stuart and Häusser, 2001; Bernard and Johnston, 2003). If the increased calcium influx that we observed during up states results from boosting of AP backpropagation, one might therefore expect that (1) the effect would be more pronounced in distal than in proximal regions of the apical dendrite, and (2) distal (but not proximal) calcium influx would be increased by synaptic input regardless of whether it is accompanied by a prolonged depolarization, such as occurs during an up state.

To test the first of these predictions, we measured AP-evoked dendritic calcium transients in the proximal apical trunk, 50–100 μm from the soma (Fig. 8*A*). The peak amplitude of these proximal calcium transients was independent of the prestimulus membrane potential (Fig. 8*B*) (slope not significantly different from zero in all five neurons examined, $p > 0.25$; Spearman rank correlation). The mean amplitude during up states was 102 ± 1% of that evoked by current injection during down states ($n = 5$ neurons) (Fig. 8*C*). As in the neurons with distal measurements, neither AP amplitudes nor halfwidths were significantly different between up and down states ($p > 0.4$; Mann–Whitney *U* test).

Comparing proximal and distal measurements, the enhancement of calcium influx with depolarization was greater at all distal locations than in any proximal location (Fig. 9*A*). On average, amplitudes in the proximal dendrite increased with a slope of 0.09% $\Delta F/F$ per millivolt of depolarization, whereas a steeper slope of 0.5% $\Delta F/F$ per millivolt of depolarization was observed in the distal dendrite (Fig. 9*B*). This is consistent with sodium channel-dependent boosting of AP amplitude by synaptic activity in the distal dendrite.

To test the second prediction we evoked synaptic input during down states using extracellular stimulation through a tungsten electrode placed in layer 1. Stimulus strength was just sufficient to evoke a single AP. Two sources of evidence indicate that extracellularly evoked APs initiated in the axosomatic region and backpropagated into the apical dendrite rather than initiating in the dendrite and propagating toward the soma. First, APs evoked by

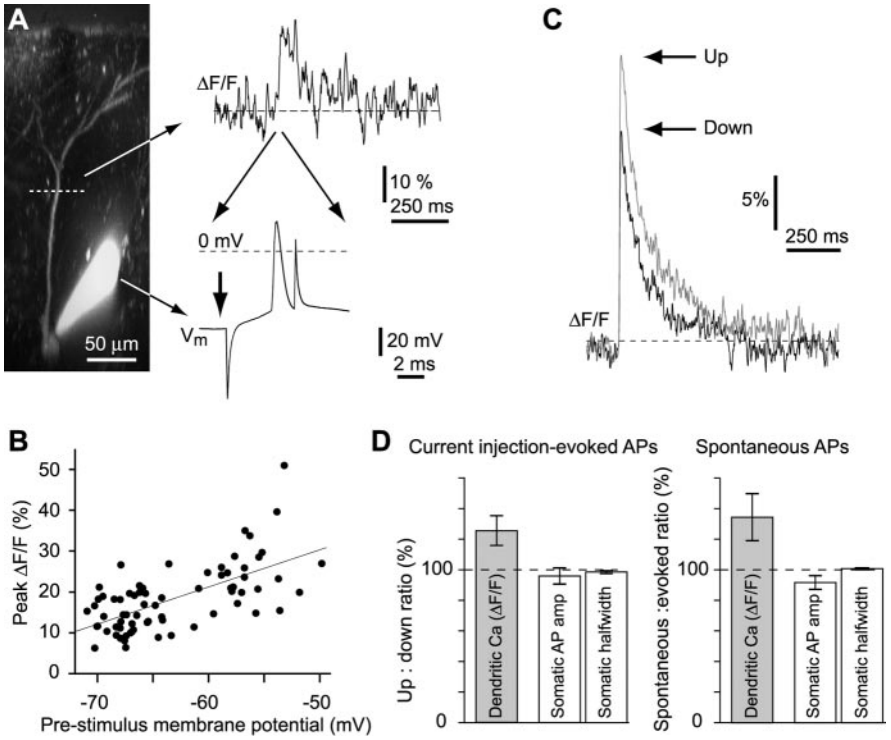

Figure 6. AP-evoked dendritic calcium influx is enhanced by synaptic activity. *A,* Left, Two-photon side projection of an L2/3 neuron and the somatic recording pipette. Right, An example of a single AP evoked by somatic current injection and the resulting dendritic calcium transient (line scan position marked on image). The arrow on the V_m trace indicates the prestimulus membrane potential. *B,* Plot of peak AP-evoked relative fluorescence change as a function of the prestimulus membrane potential for the neuron shown in *A*. Each point represents a single trial. *C,* Mean single AP-evoked calcium transients during up and down states for the neuron shown in *A*. *D,* Left, Mean ± SEM data for four neurons. Dendritic calcium measurements were made in the distal apical trunk, 150–175 μm from the soma. Peak AP-evoked dendritic calcium influx during up states was normalized to the AP-evoked influx during down states (gray bar). The ratio of somatic AP amplitude and halfwidth during up and down states for the same four neurons is also shown. Right, Similar data for spontaneous APs, normalized to APs evoked by current injection during down states ($n = 3$ neurons). Dendritic calcium measurements were made 110–160 μm from the soma.

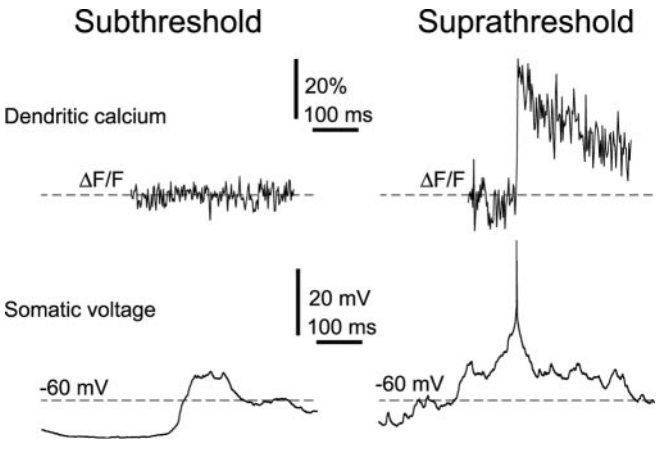

Figure 7. Absence of calcium influx during subthreshold up states. Somatic recordings (bottom) and dendritic calcium measurements (top) for subthreshold up states (left) and for spontaneous APs (suprathreshold up states; right) are shown. Data are the means of four (suprathreshold) and 15 (subthreshold) trials from a single neuron. The dendritic measurement site was in the apical trunk, 160 μm from the soma. Note that the AP amplitude is truncated.

extracellular stimulation had a similar shape to APs evoked by somatic current injection (Fig. 10*A*). The shape of APs that initiate in the dendritic tree is sufficiently different that they are readily distinguished from somatically initiated APs (in slice preparations; M. Larkum, J. Waters, B. Sakmann, and F. Helmchen, unpublished observation). Second, APs evoked by extracellular stimulation produced a spatial profile of calcium influx similar to that from APs evoked by current injection, with a maximum amplitude calcium influx in the proximal trunk and a decline toward the distal dendrite (supplemental Fig. 1, available at www.jneurosci.org as supplemental material).

We evoked synaptically driven APs by extracellular stimulation during down states, i.e., in the absence of the prolonged depolarization of an up state. As predicted, calcium influx into the distal dendrite (150–200 μm from the soma) was greater for extracellularly evoked APs than for APs evoked by current injection during down states (by 57 ± 8%; significantly larger influx in three of four neurons, $p < 0.01$; Mann–Whitney *U* test) (Fig. 10*A,B*). In contrast, in the proximal dendrite (50–100 μm from the soma) extracellularly evoked APs produced similar or slightly less calcium influx than APs evoked by current injection during down states (13 ± 8% reduction, not significantly different in three of five cells, $p > 0.01$; Mann–Whitney *U* test).

Extracellularly evoked APs occurred with a short latency (from the onset of stimulation to threshold: 5.5 ± 0.9 msec; range, 2.5–8.2 msec). Hence, enhanced calcium influx occurs only in the distal dendrite and requires only a few milliseconds of depolarization before the AP. These results are consistent with AP boosting by evoked synaptic input.

Discussion

Here we have shown that spontaneous, subthreshold up–down fluctuations occur simultaneously throughout L2/3 pyramidal neurons, with similar amplitudes in the soma, apical trunk and tuft dendrites. Spontaneous activity of this type and evoked synaptic activity both enhance dendritic calcium influx during a backpropagating AP. This enhancement is restricted to the distal apical dendrite and requires only brief synaptic input. Together these findings indicate that enhanced calcium influx results from boosting of AP backpropagation, where synaptic input activates dendritic sodium channels and/or inactivates dendritic potassium channels. This reduces the decrement of AP amplitude during backpropagation. As a consequence, during up states APs reach further into the apical dendritic tree, extending the spatial profile of calcium influx toward distal dendritic regions (Fig. 10*C*) (supplemental Fig. 1, available at www.jneurosci.org as supplemental material) and strengthening retrograde signaling from the soma to the dendrites.

Cortical up states are driven by synaptic activity throughout the local cortical network, causing near-simultaneous somatic depolarization in many neurons (Lampl et al., 1999; Petersen et al., 2003). The origin of this synaptic input is unclear, but may include both corticocortical and subcortical afferents. The distri-

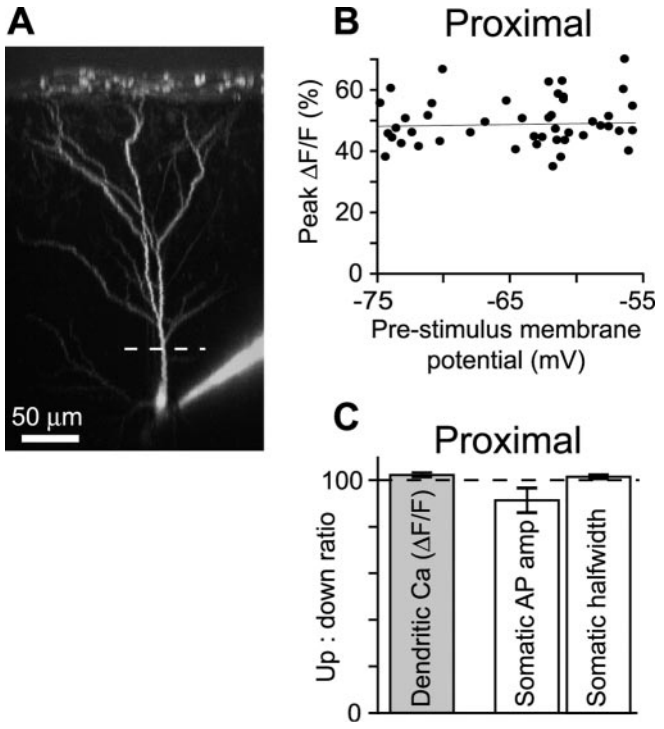

Figure 8. Calcium influx is not enhanced in the proximal dendrite. *A,* Two-photon side projection of an L2/3 neuron showing the linescan location, 50 μm from the soma (dashed line). *B,* Plot of peak AP-evoked relative fluorescence change in the proximal dendrite as a function of the prestimulus membrane potential for the neuron shown in *A*. *C,* Mean ± SEM data for four neurons. Dendritic calcium measurements were made in the proximal apical trunk, 50–100 μm from the soma. Peak AP-evoked dendritic calcium influx during up states was normalized to the AP-evoked influx during down states (gray bar). The ratio of somatic AP amplitude and halfwidth during up and down states for the same four neurons is also shown.

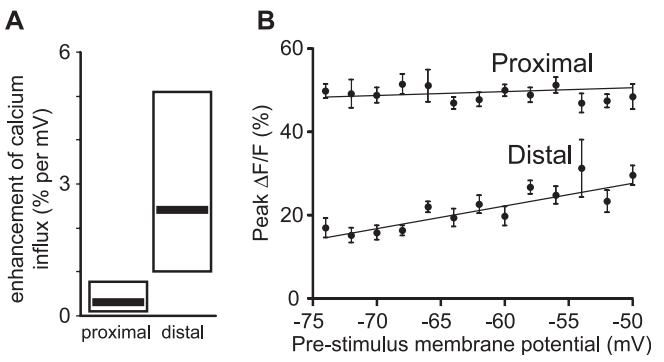

Figure 9. Comparison of mean calcium influx in proximal and distal dendrites. Pooled data summarizing the enhancement of calcium influx with depolarization in proximal and distal locations are shown. *A,* Mean (thick lines) and range of the slopes of the relationship between calcium transient amplitudes and prestimulus membrane potential for proximal (50–100 μm from the soma; $n = 4$) and distal (150–175 μm from soma; $n = 4$) measurements. Enhancement is expressed as a percentage increase in the amplitude of the calcium transient per millivolt of depolarization. Note that the data fall into two discrete groups. *B,* A comparison of the effects of synaptic activity (measured as prestimulus membrane potential) on the amplitudes of AP-evoked dendritic calcium transients for both proximal and distal measurements. Each point represents the mean ± SEM. Unconstrained linear fits had slopes of 0.09 and 0.5% $\Delta F/F$ per millivolt for proximal and distal data, respectively.

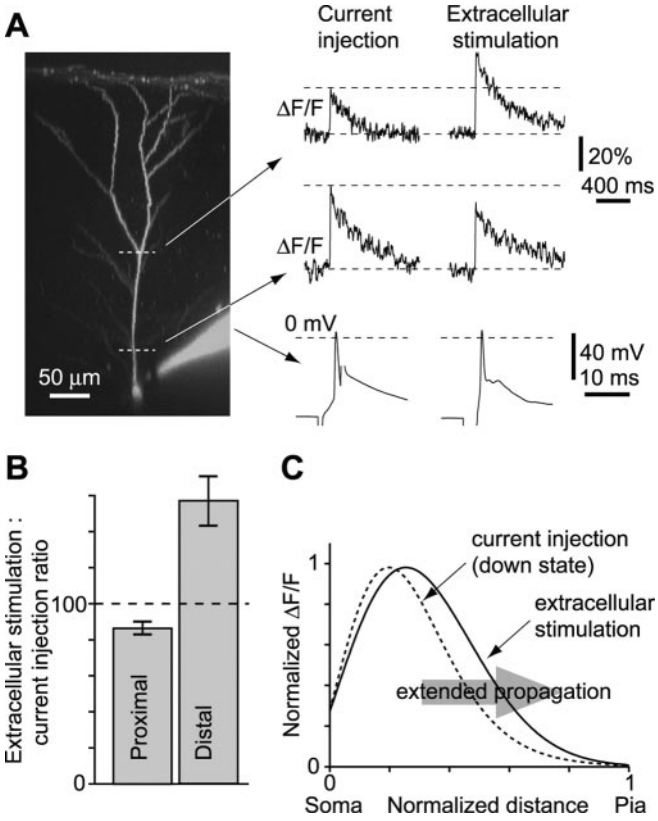

Figure 10. Dendritic calcium influx during evoked synaptic input. *A,* Left, Two-photon side projection of an L2/3 neuron showing proximal and distal linescan locations (50 and 175 μm from soma, respectively). Right, Comparison of dendritic calcium transients after APs evoked by current injection (left column) and by extracellular stimulation (right column; stimulus, 300 μA, 1 msec). Bottom row, Electrical recordings from the somatic electrode (capacitance transients truncated). Top and middle rows, Calcium transients from the distal and proximal dendritic locations. *B,* Mean ± SEM amplitudes of calcium transients evoked by extracellular stimulation normalized to those evoked by current injection during down states (proximal, $n = 4$; distal, $n = 5$). *C,* Summary of the boosting effect of extracellularly evoked synaptic activity. The normalized spatial profiles of calcium influx along the apical dendrite evoked by single back-propagating APs are shown for current injection (dashed line) and for extracellular stimulation (solid line). Both curves are skewed Gaussian fits to calcium transient amplitudes as a function of normalized distance from the soma (supplemental Fig. 1, available at www.jneurosci.org as supplemental material). The spatial profile for APs evoked by current injection is taken from our previous work (Waters et al., 2003).

bution of these afferents over the dendritic tree is not uniform. For instance, long-range feedback connections from secondary somatosensory areas arrive principally via synapses in L1 (Cauller and Connors, 1994; Cauller et al., 1998). Because up states are presumably driven by a subset of the many synaptic inputs onto a neuron, one might expect up state amplitudes to differ in different parts of the neuron. We have shown that this is not the case; up states are of similar amplitude throughout the apical dendrite. Furthermore, during up states spectral power increased across all frequencies both at the soma (as reported previously; Stern, Kincaid and Wilson, 1997) and in the dendrite. In addition, high-frequency components were particularly prominent in dendritic recordings. Together these findings point to the presence of distal synaptic input.

We found that up states occur synchronously at the soma and in the dendritic tuft. We reached this conclusion via comparison of the single-cell membrane potential with a surface electrocorticogram measurement. The electrocorticogram and electroencephalogram are thought to arise from synchronized synaptic potentials in dendrites near the cortical surface (Martin, 1991). Our data provide direct evidence for this.

It has been suggested that "background" synaptic activity

would suppress AP backpropagation *in vivo* (Steriade, 2001a,b; Rudolf and Destexhe, 2003; but see also Buzsaki and Kandel, 1998; Kerr and Plenz, 2002; Charpak et al., 2001). Our data indicate otherwise; we found that both spontaneous and evoked activity enhance AP-evoked calcium influx into the distal dendrite. If the amplitudes of backpropagating APs were reduced, this would lead to reduced, rather than enhanced calcium influx. Hence, our results indicate that AP backpropagation is not suppressed by synaptic activity. Furthermore, this enhancement is restricted to the distal dendrite and occurs rapidly with synaptic input.

There are a number of potential mechanisms for the increased distal calcium influx. We consider several of them unlikely. First, synaptically driven calcium influx, through calcium channels or ionotropic receptors, might add to AP-evoked calcium influx. For example, in striatal spiny neurons NMDA receptor-dependent enhancement of AP-evoked calcium influx occurs during up states (Kerr and Plenz, 2004). In these neurons, widespread dendritic calcium transients occur even during subthreshold up states (Kerr and Plenz, 2002), and AP-evoked calcium influx is enhanced throughout the dendritic tree (Kerr and Plenz, 2004). In contrast, in our experiments subthreshold synaptic input did not produce a calcium signal in the apical trunk, although it presumably caused localized calcium influx at active dendritic spines (Kovalchuk et al., 2000; Sabatini et al., 2002). In addition, the lack of enhanced calcium influx in the proximal dendrite is inconsistent with a widespread contribution from synaptic calcium influx. A contribution from NMDA receptors is therefore unlikely.

Second, changes in the modulatory state and availability of distal calcium channels are unlikely mechanisms. Unlike in hippocampal pyramidal neurons (Christie et al., 1995; Magee and Johnston, 1995) the densities and distributions of calcium channel subtypes have not been characterized in L2/3 neurons. We therefore cannot exclude the possibility that distal dendritic channels are more sensitive to predepolarization than those in the proximal dendrite. However, neuromodulatory effects and changes in the available pool of calcium channels would both require longer activation than the few milliseconds available in our experiments during the onset of an evoked synaptic potential (Dolphin, 1996; Perez-Reyes, 2003).

We cannot unequivocally rule out alternative mechanisms, but the most likely mechanism for the enhanced distal calcium influx is the boosting of backpropagating APs by synaptically driven depolarization, as described in hippocampal and neocortical L5 pyramidal neurons in slice preparations (Magee and Johnston, 1997; Stuart and Häusser, 2001). This could occur through either increased activation of sodium channels or inactivation of potassium channels. In hippocampal neurons, A-type potassium channels inactivate more rapidly than sodium channels. Hence, subthreshold depolarization can boost AP backpropagation through suppression of potassium channels (Pan and Colbert, 2001). In contrast, A-type channels have been excluded as a mechanism for EPSP-dependent boosting in L5 pyramidal neurons *in vitro* (Stuart and Häusser, 2001). Because little is known about dendritic channels in L2/3 neurons, it is unclear whether AP boosting results from increased sodium channel activation or potassium channel inactivation (or both) in these neurons.

What, exactly, do we mean by 'boosting?' We have previously shown that AP backpropagation in the apical dendrite of L2/3 neurons is actively supported by sodium channels, both *in vitro* and during down states *in vivo* (Waters et al., 2003). However, AP amplitude declines progressively during backpropagation along the dendrite. This is similar to L5 and hippocampal pyramidal neurons, where the AP amplitude eventually drops below the activation threshold for sodium channels as it propagates along the dendrite. AP spread is passive beyond this transition point (Stuart and Häusser, 2001; Bernard and Johnston, 2003). In hippocampal neurons, this point is ~260 μm from the soma (Bernard and Johnston, 2003). The location of the transition point in L2/3 neurons is unknown, but the decline in AP amplitude is steeper than in hippocampal neurons, so the transition point is probably significantly closer to the soma than 260 μm. The transition point may therefore be close to the location where our calcium measurements were made, 150–200 μm from the soma. Hence, the enhanced calcium influx in the distal dendrite could result from either linear or supralinear summation of AP and EPSP, which would occur in those regions of dendrite supporting active and passive propagation, respectively (Stuart and Häusser, 2001; Bernard and Johnston, 2003).

We thus use the term "boosting" inclusively, to encompass both linear and supralinear summation. Our data are consistent with either mechanism because both will result in an increased AP amplitude, either might have a more pronounced effect on dendritic calcium influx in the distal than in the proximal dendrite, and both would occur on the time scale of a single EPSP. Whether the boosting that we have observed results from linear or supralinear summation of EPSP, and AP has no bearing on our principal conclusion, that AP amplitude is increased, resulting in stronger activation of calcium channels.

In a previous study, we described an example of supralinear summation of AP and EPSP in the distal dendrite *in vitro* (Waters et al., 2003). This resulted in an even stronger distal extension of the spatial profile of calcium transients than we have described here. In the previous experiments, the combined dendritic depolarization of a backpropagating AP and an EPSP probably evoked a dendritically initiated spike. In the current *in vivo* study, we found no evidence of dendritic spikes and calcium transients were not observed in tuft dendrites. Dendritic spikes are exquisitely sensitive to inhibition in brain slices (Larkum et al., 1999) and may occur only under certain conditions *in vivo*, perhaps when GABAergic activity is suppressed.

In conclusion, AP backpropagation into the apical dendrite is not suppressed during synaptic activity. In fact it is stronger than in slice preparations and during down states *in vivo*. Extended backpropagation is likely to represent the physiological strength of backpropagation because APs necessarily coincide with synaptic activity *in vivo*. Backpropagation in the absence of synaptic activity, as typically observed in slice preparations, should perhaps be regarded as slightly suppressed. High levels of synaptic activity also occur during wakefulness (Steriade et al., 2001; Destexhe et al., 2003). Based on our findings, we expect backpropagation in the awake animal to be promoted rather than suppressed. Hence, spike patterns in pyramidal neurons would be reliably reported to the dendrites in the awake animal. Action potentials can thereby serve as a feedback signal for timing-dependent synaptic modification (Magee and Johnston, 1997; Sjöström and Nelson, 2002) or enable association between superficial and deep-layer inputs (Larkum et al., 1999) Our findings support the idea that active dendritic properties have a major impact on synaptic integration, not only during sleep-like states, but also in awake animals.

References

Bernard C, Johnston D (2003) Distance-dependent modifiable threshold for action potential back-propagation in hippocampal dendrites. J Neurophysiol 90:1807–1816.

Brecht M, Roth A, Sakmann B (2003) Dynamic receptive fields of reconstructed pyramidal cells in layers 3 and 2 of rat somatosensory barrel cortex. J Physiol (Lond) 553:243–265.

Buzsaki G, Kandel A (1998) Somadendritic backpropagation of action potentials in cortical pyramidal cells of the awake rat. J Neurophysiol 79:1587–1591.

Cauller LJ, Connors BW (1994) Synaptic physiology of horizontal afferents to layer I in slices of rat SI neocortex. J Neurosci 14:751–762.

Cauller LJ, Clancy B, Connors BW (1998) Backward cortical projections to primary somatosensory cortex in rats extend long horizontal axons in layer I. J Comp Neurol 390:297–310.

Charpak S, Mertz J, Beaurepaire E, Moreaux L, Delaney K (2001) Odor-evoked calcium signals in dendrites of rat mitral cells. Proc Natl Acad Sci USA 98:1230–1234.

Christie BR, Eliot LS, Ito K, Miyakawa H, Johnston D (1995) Different Ca^{2+} channels in soma and dendrites of hippocampal pyramidal neurons mediate spike-induced Ca^{2+} influx. J Neurophysiol 73:2553–2557.

Cowan RL, Wilson CJ (1994) Spontaneous firing patterns and axonal projections of single corticostriatal neurons in the rat medial agranular cortex. J Neurophysiol 71:17–32.

Destexhe A, Rudolph M, Paré D (2003) The high-conductance state of neocortical neurons in vivo. Nat Rev Neurosci 4:1–13.

Dolphin AC (1996) Facilitation of Ca^{2+}current in excitable cells. Trends Neurosci 19:35–43.

Häusser M, Spruston N, Stuart GJ (2000) Diversity and dynamics of dendritic signaling. Science 290:739–744.

Helmchen F, Waters J (2002) Ca^{2+} imaging in the mammalian brain in vivo. Eur J Pharmacol 447:119–129.

Johnston D, Wu SM-S (1995) Extracellular field recordings. In: Foundations of cellular neurophysiology, pp 423–440. Cambridge, MA: MIT.

Kerr JN, Plenz D (2002) Dendritic calcium encodes striatal neuron output during up-states. J Neurosci 22:1499–1512.

Kerr JN, Plenz D (2004) Action potential timing determines dendritic calcium during up-states. J Neurosci 24:877–885.

Kovalchuk Y, Eilers J, Lisman J, Konnerth A (2000) NMDA receptor-mediated subthreshold Ca^{2+} signals in spines of hippocampal neurons. J Neurosci 20:1791–1799.

Lampl I, Reichova I, Ferster D (1999) Synchronous membrane potential fluctuations in neurons of the cat visual cortex. Neuron 22:361–374.

Larkum ME, Zhu JJ, Sakmann B (1999) A new cellular mechanism for coupling inputs arriving at different cortical layers. Nature 398:338–341.

Lübke J, Egger V, Sakmann B, Feldmeyer D (2000) Columnar organization of dendrites and axons of single and synaptically coupled excitatory spiny neurons in layer 4 of the rat barrel cortex. J Neurosci 20:5300–5311.

Magee JC, Johnston D (1995) Characterization of single voltage-gated Na^+ and Ca^{2+} channels in apical dendrites of rat CA1 pyramidal neurons. J Physiol (Lond) 487.1:67–90.

Magee JC, Johnston D (1997) A synaptically controlled, associative signal for Hebbian plasticity in hippocampal neurons. Science 275:209–213.

Margrie TW, Brecht M, Sakmann B (2002) In vivo, low-resistance, whole-cell recordings from neurons in the anaesthetized and awake mammalian brain. Pflügers Arch 444:491–498.

Martin JH (1991) The collective electrical behavior of cortical neurons: the electroencephalogram and the mechanisms of epilepsy. In: Principles of neural science (Kandel ER, Schwartz JH, Jessell TM, eds), pp 777–791. Norwalk, CT: Appleton and Lange.

Migliore M, Shepherd GM (2002) Emerging rules for the distributions of active dendritic conductances. Nat Rev Neurosci 3:362–370.

Pan E, Colbert CM (2001) Subthreshold inactivation of Na^+ and K^+ channels supports activity-dependent enhancement of back-propagation action potentials in hippocampal CA1. J. Neurophysiol 85:1013–1016.

Perez-Reyes E (2003) Molecular physiology of low-voltage-activated T-type calcium channels. Physiol Rev 83:117–161.

Petersen CCH, Hahn TTG, Mehta M, Grinvald A, Sakmann B (2003) Interaction of sensory responses with spontaneous depolarization in layer 2/3 barrel cortex. Proc Natl Acad Sci USA 100:13638–13643.

Reyes A (2001) Influence of dendritic conductances on the input-output properties of neurons. Annu Rev Neurosci 24:653–675.

Rudolf M, Destexhe A (2003) A fast-conducting, stochastic integrative mode for neocortical neurons *in vivo*. J Neurosci 23:2466–2476.

Sabatini BL, Oertner TG, Svoboda K (2002) The life cycle of Ca^{2+} ions in dendritic spines. Neuron 33:439–452.

Sjöström PJ, Nelson SB (2002) Spike timing, calcium signals and synaptic plasticity. Curr Opin Neurobiol 12:305–314.

Steriade M (2001a) Impact of network activities on neuronal properties in corticothalamic systems. J Neurophysiol 86:1–39.

Steriade M (2001b) Similar and contrasting results from studies in the intact and sliced brain. In: The intact and sliced brain, pp 134–142. Cambridge, MA: MIT.

Steriade M, Nunez A, Amzica F (1993) A novel slow ($<$1 Hz) oscillation of neocortical neurons *in vivo*: depolarizing and hyperpolarizing components. J Neurosci 13:3252–3265.

Steriade M, Timofeev I, Grenier F (2001) Natural waking and sleep states: a view from inside neocortical neurons. J Neurophysiol 85:1969–1985.

Stern EA, Kincaid EA, Wilson CJ (1997) Spontaneous subthreshold membrane potential fluctuations and action potential variability of rat corticostriatal and striatal neurons in vivo. J Neurophysiol 77:1697–1715.

Stuart G, Sakmann B (1994) Active propagation of somatic action potentials into neocortical pyramidal cell dendrites. Nature 367:69–72.

Stuart GJ, Häusser M (2001) Dendritic coincidence detection of EPSPs and action potentials. Nat Neurosci 4:63–71.

Stuart G, Schiller J, Sakmann B (1997a) Action potential initiation and propagation in rat neocortical pyramidal neurons. J Physiol (Lond) 505:617–632.

Stuart G, Spruston N, Sakmann B, Häusser M (1997b) Action potential initiation and backpropagation in neurons of the mammalian CNS. Trends Neurosci 20:125–131.

Svoboda K, Denk W, Kleinfeld D, Tank DW (1997) In vivo dendritic calcium dynamics in neocortical pyramidal neurons. Nature 385:161–165.

Svoboda K, Helmchen F, Denk W, Tank DW (1999a) Spread of dendritic excitation in layer 2/3 pyramidal neurons in rat barrel cortex in vivo. Nat Neurosci 2:65–73.

Svoboda K, Tank DW, Stepnowski RA, Denk W (1999b) Two-photon imaging of neuronal function in the neocortex in vivo. In: Imaging neurons (Yuste R, Konnerth A, Lanni F, eds), pp 22.1–22.11. Cold Spring Harbor, NY: Cold Spring Harbor.

Timofeev I, Grenier F, Steriade M (2001) Disfacilitation and active inhibition in the neocortex during the natural sleep-wake cycle: an intracellular study. Proc Natl Acad Sci USA 98:1924–1929.

Tsubokawa H, Ross WN (1996) IPSPs modulate spike backpropagation and associated $[Ca^{2+}]_i$ changes in the dendrites of hippocampal CA1 pyramidal neurons. J Neurophysiol 76:2896–2906.

Waters J, Larkum M, Sakmann B, Helmchen F (2003) Supralinear Ca^{2+} influx into dendritic tufts of layer 2/3 neocortical pyramidal neurons *in vitro* and *in vivo*. J Neurosci 23:8558–8567.

Waters J, Schaefer A, Sakmann B (2005) Backpropagating action potentials in neurones: measurement, mechanisms and potential functions. Prog Biophys Mol Biol 87:145–170.

Xiong W, Chen WR (2002) Dynamic gating of spike propagation in the mitral cell lateral dendrite. Neuron 34:115–126.